Long-Term Hyperglycemia Induces α-Synuclein Aggregation and Dopaminergic Neuronal Loss in Parkinson's Disease Mouse Model

Yi-Qing Lv
China Medical University
Lin Yuan
China Medical University
Yan Sun
China Medical University
Hao-Wen Dou
China Medical University
Ji-Hui Su
China Medical University
Zhi-Pan Hou
China Medical University
Jia-Yi Li
Lund University
Wen Li (fox393933570@126.com)
China Medical University https://orcid.org/0000-0002-0383-0240

Research

Keywords: Hyperglycemia, diabetes mellitus, Parkinson's disease, neurodegeneration, neuroinflammation

Posted Date: October 15th, 2021

DOI: https://doi.org/10.21203/rs.3.rs-961629/v1

Abstract

Background: Growing evidence suggest the association between Parkinson's disease (PD) and diabetes mellitus (DM). On a cellular level, it was proven that long-term elevated levels of glucose might lead to nigrostriatal degeneration in PD models. However, the underlying mechanism is still unclear. Previously, we have elucidated the potential of type 2 diabetes mellitus (T2DM) in facilitating PD progression, involving aggregation of both alpha-synuclein (α-syn) and islet amyloid polypeptide (IAPP) in the pancreatic and brain tissues. However, due to the complicated effect of insulin resistance on PD onset, the actual mechanism of hyperglycemia-induced dopaminergic degeneration remains unknown.

Methods: In the present study, we employed the type 1 diabetes mellitus (T1DM) model induced by streptozotocin (STZ) injection, to investigate the direct effect of elevated blood glucose level on nigrostriatal degeneration.

Results: We found that STZ treatment induced more severe pathological alterations in the pancreatic islets and T1DM symptoms in α-syn-overexpression mice than that in wild type (WT) mice, one month and three months after STZ injections. Behavioral tests evaluating motor performance confirmed the nigrostriatal degeneration. Furthermore, we observed a marked decrease in dopaminergic profiles and an increase of α-syn accumulation and Serine 129 (S129) phosphorylation in STZ-treated α-syn mice compared with vehicle-treated mice. At last, we observed more severe neuroinflammation in the brain of the STZ-treated α-syn mice.

Conclusion: Our results solidify the potential link between DM and PD, providing insights on how hyperglycemia induces nigrostriatal degeneration and contributes to pathogenetic mechanisms in PD.

1. Background

Parkinson's disease (PD) is the second most common neurodegenerative disease after Alzheimer's disease (AD) in human, presenting mainly motor discoordination accompanied by various non-motor symptoms, such as cognitive impairments[1]. Progressive loss of dopaminergic neurons in the substantia nigra pars compacta (SNpc) and the formation of cytoplasmic inclusions, called Lewy Bodies (LBs), are the two major neuropathological hallmarks of PD[2]. LBs are primarily composed of misfolded α-syn, which plays a crucial role in PD pathogenesis[3]. The etiology of PD is not yet clear. Most PD cases are sporadic, associated with different contributing risk factors such as aging and neurotoxins, etc.[4]. Available evidence suggests that certain metabolic diseases may also serve as risk factors for PD, such as diabetes mellitus (DM)[5]. DM is a group of complex metabolic diseases characterized by impaired glucose metabolism and subsequent hyperglycemia resulting from defects in insulin secretion and efficiency[6]. Based on the concepts of being "insulin-sensitive" and "insulin-insensitive"[7], DM can be divided into type 1 diabetes mellitus (T1DM) with insufficient insulin secretion due to progressive destruction of pancreatic β cells, and type 2 diabetes mellitus (T2DM) with the lack of appropriate insulin response[8–11].

PD and DM share similarities in multiple aspects, including epidemiology, etiology and pathogenesis. First, epidemiologically, DM presents as a risk factor for PD. Both PD and DM are of multifactorial origins with high prevalence. Diabetes is among the most prevalent chronic diseases, and researchers predicted a near doubling of patients with DM by 2030 compared to figures obtained in 2000[12]. PD is a disease with an increasing prevalence in the elderlies, and the projected prevalence cases for PD are predicted to increase during the next 40 years[13]. Accumulating evidence suggests that DM constitutes a risk factor associated with increased neurodegenerative diseases[5]. The elevated risk of developing cognitive abnormalities in individuals with impaired glucose metabolism is well documented[14, 15]. Epidemiological studies indicate that patients with preexisting DM have an increased incidence of developing PD and often display parkinsonian symptoms[16–20]. Secondly, PD and DM have shared potential contributing factors and overlapping pathology. Environmental exposure, genetic susceptibility and lifestyle factors[21–23] are well-known PD and DM causal factors. Clinically, some diabetic patients exhibit pathologies related to striatal dopaminergic dysfunction[11, 24]. Furthermore, DM and PD also share common etiopathogenic features[15, 20], such as dopaminergic neuronal loss in SNpc and α-syn aggregation in the pancreatic β cells in diabetic patients[25].

Although a growing body of epidemiological and clinical data favor the association between DM and PD[26], to date, the molecular mechanisms by which elevated levels of blood glucose associates with the development of PD are still unclear. Experimental studies support the toxic role of hyperglycemia in the central nervous system (CNS)[27, 28]. Our previous study has suggested the possible role of protein co-aggregation during the interplay of the two diseases in a non-human primate model[29]. However, considering the influence of insulin resistance in amyloid protein aggregation[30], the mechanisms of hyperglycemia induced-neurodegeneration remain obscure. Of all the shared mechanisms of DM and PD, neuroinflammation has unneglectable importance. First, diabetes mediates many of its effects through inflammation. T2DM can present oxidative stress and peripheral inflammation[31]. Diabetic patients often show mild chronic inflammation, reflected by the elevation of peripheral blood cytokines such as interleukin-6 (IL-6), tumor necrosis factor-alpha (TNF-α) and interleukin-1β (IL-1β)[32, 33]. Secondly, systemic inflammatory status is associated with the interruption of blood-brain barrier (BBB) integrity. Corrupted BBB may subsequently cause leukocyte infiltration, diffusion of cytokines and entry of toxins into the CNS[34, 35], therefore trigger neuroinflammation and activate microglia[36]. At last, prolonged microglial activation is proven to be a major factor in driving dopaminergic degeneration in PD[37]. From DM to systematic inflammation, which thereafter induces neuroinflammation and then promotes the onset and progress of PD, a lot of evidence is shown to explain the mechanism of hyperglycemia-induced neurodegeneration. As a matter of fact, many studies highlight the importance of DM-induced neuroinflammation and its link to neurodegenerative diseases, such as AD[38].

Therefore, to study the effect of hyperglycemia on the nigrostriatal pathway and better understand the mechanistic connection between DM and PD, we have employed. the streptozotocin (STZ) induced-T1DM model in the background of both wild type (WT) and α-syn transgenic mice. After characterizing the T1DM phenotypes, we investigated PD related features in the mice regarding motor dysfunction, dopaminergic neuron and terminal loss, and α-syn aggregation. We found that intraperitoneal injection

(i.p.) of STZ exacerbated degeneration of dopaminergic neurons in the α-syn-overexpression mice, which were accompanied by an increase in α-syn aggregation and phosphorylation. Moreover, we observed markedly increased neuroinflammation in the nigrostriatal systems of STZ-injected α-syn mice, suggesting the potential mechanistic role of neuroinflammation connecting hyperglycemia and the subsequent PD-related alternations.

2. Materials And Methods

2.1. Animals

BAC-α-syn-GFP mice and the C57 black 6 (C57BL/6) mice from 11-12 weeks of age were used to generate STZ-induced diabetic models. The BAC-α-syn-GFP mouse model has been described previously[39–41]. Briefly, the transgenic mice express human WT full-length α-syn fused with green fluorescent protein (GFP) under mouse α-syn gene promoter, generated by pronuclear inoculation of bacterial artificial chromosome (BAC) to C57BL/6 background. Mice were housed (4 to 6 animals per cage) under standard laboratory conditions (a strict 12/12-h light-dark cycle with food and water supplied *ad libitum*) in a temperature-controlled (25°C) facility. All housing, breeding and animal experiment procedures were approved by the Research Ethics Committee of China Medical University and performed according to the international guidelines.

2.2. Animal grouping

BAC-α-syn-GFP mice and WT mice were randomly allocated to four different groups: (1) BAC-α-syn-GFP mice with sodium citrate buffer treatment (α-syn-vehicle) (2) BAC-α-syn-GFP mice with STZ treatment (α-syn+STZ) (3) WT mice with sodium citrate buffer (WT-vehicle) (4) WT mice with STZ treatment (WT+STZ). Each group was divided into short-term (one month after injection) and long-term (three months after injection) for subsequent studies.

2.3. Induction of T1DM with STZ

Both BAC-α-syn-GFP mice and C57BL/6 mice were given low-dose STZ (Sigma-Aldrich S0130) for 5 consecutive days[42]. Food deprivation was performed 16 h prior to STZ treatment. STZ compound was dissolved in 0.1 mol/L sodium citrate buffer (pH 4.5) and injected i.p. with 70 mg/kg of body weight within 15 min of dissolution, once per day. The vehicle group received an equal volume of citrate buffer without STZ correspondingly.

2.4. Evaluation of blood glucose and body weight

Body weights and blood glucose were measured on day 0, 7, 14, 28, 49 and 84 after STZ injection. Blood was collected from tail veins for glucose determinations, using an electronic scale (YuWell, China) following fasting for 12 h (Fig. 1A). The mice were then re-fed. Animals with random blood glucose value >150 mg/dL (8.3 mmol/L) were defined as successfully induced diabetic mice.

2.5. Behavioral tests

Pole Test. Pole test was used to assess the motor coordination and balance of mice before sacrifice. Based on previously published methods[43], a steel pipe with the length of 55 cm and diameter of 1 cm was tightly wrapped in white antiskid gauze and fixed on plastic foam base. A spherical protrusion with the diameter of 2 cm was placed on top of the pipe as attachment points for mice. During the experiment, mice were put on the spherical protruding point with heads upward. The time of the heads to turn down (T-turn) and the total time (T-total) of mice to climb down the pole was recorded. Average value of 5 repeated tests (minimum 3-min interval) was used for statistical analyses.

Open Field Test. Open field test was used to assess anxiety and spontaneous activity of mice as previously described[44]. Briefly, mice were placed in the test room for an hour to adapt to the surroundings. Mice were put in the center of an open field (90-cm long, 90-cm wide, and 40-cm high, divided into 9 squares) and monitored for 15 min by an overhead digital camera connected to an automated video-tracking system (Harvard Apparatus, model: SMART® v 3.0). To avoid interference from the odors left by the last mouse, the inner wall and bottom surface of the field was thoroughly wiped with 75% ethyl alcohol in between each measurement. The mean speed in the total zone, the total distance, distance in the center zone and distance in the periphery zone of mice were recorded.

2.6. Sample Collection and Processing

Mice were deeply anaesthetized with sodium pentobarbital (Apoteksbolaget, Sweden) and sacrificed by trans-cardinal perfusion with 4% paraformaldehyde (PFA). Brains were rapidly removed, kept in 4% PFA solution overnight and stored in 30% sucrose solution. 30-μm-thick coronal sections were cut and kept in anti-freeze medium (30% sucrose containing 20% ethylene glycol and 0.05% sodium azide in 0.1 M PBS) at -20°C. Pancreatic tissues were fixed in 4% PFA at 4°C for 24 h. Following dehydration with an ascending gradient of ethanol and xylene, tissues were embedded in paraffin and sectioned into 5-μm-thick slices encompassing the islets, using a rotary microtome (RM2016; Leica Microsystems GmbH). Fresh brain tissues were also collected and stored at -80°C for Western blot assessment.

2.7. Immunohistochemistry

After washing, antigen retrieval of the brain sections was performed in citrate acid buffer (pH 6.0) at 80°C for 30 min. Sections were then quenched with peroxidase solution (3% H2O2 in 10% methanol) for 15 min before blocking in 5% normal goat or house serum diluted with 0.5% TritonX-100-PBS for 1 h. Primary antibody incubation (Table S1) was performed at 4°C overnight followed by washing and incubation with biotinylated secondary antibodies. After 30-min ABC (Vector Laboratories, Cat. # VEPK-6100) incubation at room temperature, the sections were developed with 0.03% diaminobenzidine (DAB) in 0.05 M Tris-HCl (pH 7.5) for 2 min. The sections were then dehydrated and mounted with neutral balsam for microscopic analyses. Paraffin-embedded pancreatic sections were first deparaffinized with xylene and decreasing concentrations of ethanol before subjected to antigen retrieval. The quantification of

immunohistochemistry was performed using the Image J software (version 1.34.3.67; National Institutes of Health) analyses.

2.8. Immunofluorescence

After antigen retrieval, brain sections were incubated in blocking solution (5% normal goat serum and 0.5% TritonX-100-PBS) at room temperature for 2 h. Primary antibody (Supplementary Table 1) incubation was performed at 4°C overnight and fluorescent secondary antibodies were applied for 2 h at room temperature, before staining with 2-(4-Amidinophenyl)-6-indolecarbamidine dihydrochloride (DAPI) (Beyotime, C1005). Thereafter, sections were mounted with an anti-fading medium for confocal analyses (Leica TCS SP8).

2.9. Western blot

Mouse brain substantia nigra (SN) tissues were fully immersed in ice-cold lysis buffer (Beyotime) containing 1% protease inhibitor cocktail and phenylmethylsulfonyl fluoride (PMSF) (Beyotime) and homogenized by ultrasonic crashing. 10 μg of total protein was loaded from each sample. SDS-PAGE were performed for 75 min at 120 V followed by transfer onto polyvinylidene difluoride membranes (PVDF) (Millipore) for 120 min at 200 mA. After blocked in 5% skimmed milk (Millipore) in TBS with 0.05% Tween-20 (TBST), the membranes were incubated with primary antibodies overnight at 4°C and horseradish peroxidase (HRP) conjugated antibodies (ECL Rabbit IgG, #NA934; ECL Mouse IgG, #NA931; GE Life Sciences) at room temperature for 1 h. Detection was enhanced by ECL kits (#180–5001, Tanon) and developed with chemiluminescence imaging analysis system (Tanon 5500). Bands were analyzed using Image J software.

2.10. Quantification

Stereological cell counting. Unbiased quantification of the total number of tyrosine hydroxylase (TH) and serine 129 phosphorylated α-syn (pS129-α-syn) positive neurons in SN were calculated according to the optical fractionator principle[45], using a stereological system including 2-dimensional anatomical mapping and cell quantification program (Stereo Investigator, MBF Bioscience, USA) coupled to a color brightfield microscope (Nikon M 570E). A full series of sections (6 sections) per mouse was used to count. The virtual outlines of the right and left SN were drawn in a manner consistent with the description provided by previous article[46]. Stereo Investigator's Virtual Slice module was used to draw interesting counting regions at low magnification. Starting at a random field, the number of stained neurons were counted under high magnification (100X objective).

The total numbers of TH-positive and pS129-α-syn-positive neurons in the SN were calculated according to the following equation:

$$N = 1/SSF \times 1/ASF \times 1/TSF \times \sum Q^{-}$$

N stands for the number of the target neurons. SSF represents the section sampling fraction. ASF means the area of sampling fraction and HSF is the thickness of sampling fraction. TSF was calculated as

dissector height/mean thickness and ∑Q⁻ was the number of neurons counted. For this investigation, SSF=6 and ASF=60%. The Gundersen coefficient of error (CE) was used to determine sufficiency of the samples (CE < 0.1).

The counting point of a neuron is appointed where the nuclear membrane was in sharp relief while focusing up and down in the z-axis, when the estimated center of the nuclei was within the counting frame and contour lines simultaneously, without touching the counting-frame line or contour line in the xy-axis.

Quantification of islet β-cell area. The area of islet β-cell area was quantified with insulin staining. Five different islet structures in at least three mice in each group were included. The area measurements of the whole islet and insulin positive tissues was determined by the Image J software (version 1.34.3.67; National Institutes of Health) analyses. The average ratio of insulin positive area in the whole islet (insulin+/islet area%) was employed to evaluate the damage of pancreatic tissues.

Quantification of microglia. For the microglia quantification, eight optical fields of high magnification (40X objective) were taken from each SN. The number of microglia was counted using the manual cell counting marker function of the Image J software. Morphological grading of microglia was performed using a standard published previously[47]. Briefly, microglia were graded based on the length and thickness of their processes, the characteristics of their cell body and the look of the nucleus, into four stages. The fluorescence co-localization between the major histocompatibility complex Class II (MHC class II) and ionized calcium binding adapter molecule 1 (Iba-1) in the striatum were quantified using the Pearson's Correction with the Fiji plugin Coloc 2[40].

2.11. Statistical analysis

Statistical analysis was performed with GraphPad Prism 8 software. Three-way analysis of variance (ANOVA) and two-way ANOVA with Dunnett-t's multiple and Tukey's multiple comparisons were employed. All values were presented as the mean ± standard error of the mean (SEM). P values and statistical methods are described in figure legends.

3. Results

3.1. Body weight loss in STZ-injected mice

To evaluate the effects of STZ in inducing hyperglycemia in mice, we routinely monitored the body weight and blood glucose level. 40% (8 of 40) of the BAC-α-syn-GFP mice died due to the STZ treatments, among which three mice died within the first month after injection, and five mice died during the following two months. In contrast, only one mouse died after vehicle injection (Fig. 1B). All STZ-injected mice developed significant loss of body weight during the first two weeks post-injection. Although there was an increasing trend in all groups during the following months, the body weights of the mice with i.p. STZ (WT+STZ, α-

syn+STZ) were significantly lower than those with vehicle injection (WT-vehicle, α-syn-vehicle) (Fig. 1C). The significantly lower body weight of STZ injected groups suggested a disrupted metabolic status.

3.2. STZ treatment induced more severe hyperglycemia in α-syn-overexpression mice compared to WT ones

In the STZ treated groups, blood glucose levels increased in both WT and BAC-α-syn-GFP mice from the first week after injection and remained at high levels (Fig. 1D). In the α-syn+STZ group, the blood glucose levels ranged from 16.3-21.0 mmol/L, while the WT+STZ group exhibited blood glucose of 10.4 to 15.28 mmol/L. Interestingly, the blood glucose level of the α-syn+STZ group was significantly higher than WT+STZ in the whole experimental period (three months) (Fig. 1D). The data indicated that we successfully created the T1DM diabetic mouse model and that STZ induced more severe hyperglycemia in the α-syn-overexpression mice than in the WT ones. On the other hand, the blood glucose level remained stable in all vehicle-treated groups, with WT-vehicle mice showing 7.3-8.7 mmol/L and α-syn-vehicle mice showing 8.3-9.3 mmol/L.

3.3. STZ treatment exacerbated more severe structural damage of islets in α-syn-overexpression mice than in WT mice

A significant decrease in the insulin-positive profile was observed in STZ-injected mouse pancreases, with the average ratio between insulin-positive area and the total islet area decreased by 31.42% and 21.7% in WT mice and 39.94% and 37.89% in BAC-α-syn-GFP mice, one and three months after injection, respectively (Fig. 2A-B). Neither WT nor BAC-α-syn-GFP injected with vehicle showed decreased insulin immunoreactivity. Notably, the ratio between insulin-positive area and the islet area in pancreases of α-syn+STZ mice reduced significantly more than that of WT+STZ mice by 21.65% at three months post-injection (Fig. 2B), indicating a more severe pancreatic β cell mass loss in α-syn mice. The pathological alterations in the pancreases suggested that STZ-treated mice exhibit features reminiscent of T1DM[48]. More importantly, under the same conditions, the more severe loss of islet β-cells occurs in α-syn mice.

3.4. Long-term hyperglycemia-induced motor deficits in α-syn-overexpression mice

We performed the pole test and open field test to assess the motor performance of the STZ-injected mice to study whether and to which extent nigrostriatal degeneration might have taken place. In the pole test, both T-turn and T-total of mice in the α-syn+STZ group were significantly longer than those of the WT+STZ and vehicle-injected groups, three months after STZ injections, suggesting that hyperglycemia aggravate more dramatic motor deficits in the α-syn mice than that in the vehicle-treated mice. Moreover, it seemed that the appearance and severity of altered behaviors are associated with the length of hyperglycemia. One-month long hyperglycemia appeared not sufficient to initiate the PD like behavioral phenotypes in WT mice (Fig. 3A-B).

We also measured the spontaneous locomotor and exploratory activity of the mice in the open field test. At one month after injection, BAC-α-syn-GFP mice exhibited no significant alterations in spontaneous movement, regardless of STZ injection or not. However, we found that the mean movement speed in α-syn+STZ mice was noticeably slower than in WT-vehicle mice three months after injection (Fig. 3C). Meanwhile, the total traveled distance (including the distance in the center and periphery) was reduced compared to WT-Vehicle mice (Fig. 3D-F). Furthermore, we found that the α-syn+STZ mice traveled a shorter distance than WT+STZ mice in the central area of the open field at three months after injection (Fig. 3E), indicating that hyperglycemia increase the susceptibility of BAC-α-syn-GFP mice to develop motor impairment (more significant at three months after injection), which might be attributable to dopaminergic damage.

3.5. Long-term hyperglycemia-induced dopaminergic neuronal degeneration in α-syn-overexpression mice

To investigate whether hyperglycemia has any impacts on the nigrostriatal dopaminergic system, we specifically examined the expression of dopaminergic neuronal markers, tyrosine hydroxylase (TH), the rate-limiting enzyme of catecholamine synthesis, and dopamine transporter (DAT). We observed significant reductions of TH and DAT in the SN of α-syn+STZ mice three months post-injection, suggesting the degeneration of dopaminergic neurons (Fig. 4A-C). No difference in the expression levels of either TH or DAT in the SN of STZ-injected mice compared to vehicle-injected groups at one month after injection was observed (Fig. 4A-C). The results were further confirmed by immunohistochemical and stereological analyses, focusing on discrete dopaminergic neurons in the ventral mesencephalon, including the SNpc and the ventral tegmental area (VTA) (Fig. S1, Fig. 4D). Mice within the α-syn+STZ group displayed a significant loss of dopaminergic neurons in the SNpc compared to WT+STZ and α-syn-vehicle groups three months after induction of hyperglycemia (Fig. 4D-E). Stereological analyses also showed time-dependent neurodegeneration in α-syn+STZ groups comparing one month and three months post-injection (Fig. 4F). Furthermore, in the striatum, the decreased expression levels of TH and DAT were also observed in STZ-treated mice three months after injection (Fig. S2). The results were consistent with what we obtained in SN, indicating that long-term hyperglycemia causes damage to both dopaminergic neurons and terminals in α-syn mice.

3.6. Hyperglycemia increased α-syn phosphorylation in the nigrostriatal system

As a consequence of α-syn overexpression, the BAC-α-syn-GFP mice develop α-syn phosphorylation and aggregation in an age-dependent manner[39]. To determine whether hyperglycemia can worsen the α-syn pathology, we studied α-syn aggregation and phosphorylation in the STZ-injected mouse brains. Overall, we found significantly higher α-syn expression and phosphorylation level[49] in the SN of the BAC-α-syn-GFP mice than WT mice in both STZ- and vehicle-injected groups. Moreover, α-syn level and phosphorylation increased in α-syn-overexpression mice along time after induction of hyperglycemia, suggesting a link between hyperglycemia and the severity of α-syn pathology (Fig. 5A-C).

Immunohistochemical analyses also showed that phosphorylated α-syn positive signals were only present in the BAC-α-syn-GFP SN, while the WT mice were lack of positive signals (Fig. 5E). Notably, in stereological quantification, we observed two different types of pS129-α-syn positive profiles (Fig. 5D), one with only pS129-α-syn positive immunoreactivity but lack of visible inclusions and the other containing pS129-α-syn-positive inclusions. The proportion of neurons containing pS129-α-syn-positive inclusions significantly increased three months after injection in α-syn+STZ mice compared to the α-syn-vehicle ones (Fig. 5F-H). These results indicated that hyperglycemia exacerbates α-syn aggregation and phosphorylation.

3.7. Hyperglycemia-induced severe neuroinflammation in α-syn-overexpression mice

To investigate the potential mechanism contributing to the pathological interaction between DM and PD, we examined mouse brain tissues with microglial (Iba-1) and astroglial (glial fibrillary acidic protein, GFAP) markers.

By immunoblotting (Fig. 6A), we observed a significant increase in Iba-1 level in the SN of α-syn+STZ mice compared to the WT-vehicle mice (Fig. 6B), indicating potential microglial activation. Immunohistochemical analyses showed a significant increase of Iba-1 positive cells in α-syn+STZ groups (both one and three months after injection) in SN (Fig. 6D-E), indicating the hyperglycemia in α-syn mice induced severe neuroinflammation. No difference in Iba-1 immunoreactivity was observed in the SN in vehicle-injected groups. Morphological alterations of microglia were further analyzed. The activation degrees of microglia were divided into four stages, including I) microglia presenting small round cell body with long thin processes, II) cells with a dense soma and processes remaining thin but longer, III) cell bodies appearing enlarged and irregular in shape, with processes becoming thicker and shorter, IV) cell bodies becoming swollen and dark, merging with thickened and branched processes[47, 50] (Fig. 6F). Quantitative analyses of microglial morphology in the SN region confirmed hyperglycemia-induced microgliosis in the STZ injected BAC-α-syn-GFP mice. Stage IV cells (Stage IV were deemed highly activated microglia, showing amoeba-like morphology) constituted over 35% and 37% of the microglia population at one and three months after injection in the α-syn+STZ group, significantly higher than that of α-syn-vehicle groups (22% and 25%) at the same time point (Fig. 6G). We observed no difference in the expression levels of GFAP in the SN of STZ-injected mice compared to vehicle-injected groups at both one and three months after hyperglycemia induction (Fig. 6C).

We further examined the functional alterations of activated microglia. Microglia expressing MHC class II in the striatum were significantly increased in the α-syn+STZ group (Fig. 7A). In addition, the co-localization of MHC class II and Iba-1 was more robust in the striatum in the α-syn+STZ group than the α-syn-vehicle and WT groups (Fig. 7B, Fig. S3). The increased expression of MHC class II in microglia indicated an activated status, wherein α-syn-overexpression mice with hyperglycemia exhibited evident neuroinflammation.

4. Discussion

Although the exact etiology of PD is still to be uncovered, there exist many risk factors facilitating the onset and progress of the disease. One major risk factor of PD is the impairment of glucose metabolism[26], which may occur years before the first motor symptoms appear, suggesting the unneglectable role of hyperglycemia in initiating PD. In this study, we used a direct hyperglycemic model by inducing pancreatic islet damage using STZ to observe whether and how the elevated blood glucose affects the degeneration process of a PD (α-syn overexpression) mouse model. We treated 3-month-old BAC-α-syn-GFP mice (an α-syn transgenic mouse model), providing experimental reference value for the early diagnostic and preventing strategies of PD.

4.1. T2DM vs. T1DM-models to study the direct effect of hyperglycemia on the progression of PD

Despite some discrepancies, there have been a number of previously published papers suggesting the association between DM and PD[17, 20, 51]. Among these reports, studies on the relationship between T2DM and PD account for the majority. Indeed, the incidence rate of T2DM is much higher than that of T1DM and it shares similarities with PD in the aspects of chronic disease progress and dominant ratio in the elderlies[11, 52]. Nevertheless, insulin resistance in T2DM affects the regulation of dopaminergic transmission and maintenance of synapses in the CNS[53]. The brains of PD patients with T2DM exhibited a process analogous to peripheral insulin resistance, suggesting potential common molecular pathways. In animal models, both high-fat diets treated and leptin receptor homozygous deficiency (db/db) mice exhibited increased vulnerability to nigrostriatal neurodegeneration[51], indicating the relation between T2DM and PD again. Our previous studies on T2DM cynomolgus monkeys also indicated that T2DM might facilitate PD onset and progress by interfering with the pathological protein aggregation[29].

However, T2DM itself has complicated etiology and pathology. Both insulin insufficiency and deficiency can occur at the same time[54]. In addition, insulin resistance on its own is challenging to elucidate[53]. Therefore, it would have been rather narrow to own the T2DM induced PD disease progression to sole hyperglycemia. Despite hyperglycemia, it has been widely proven that T2DM is often accompanied by aberrations in lipid metabolism and other related metabolic abnormalities, making the disease background hard to elucidate. Diabetic dyslipidemia is often present among patients with T2DM (72-85%), while patients with T1DM usually do not have such dyslipidemia (<10%)[55, 56]. Simultaneously, such aberrations of lipid metabolism can also be observed in T2DM animal models[29, 57]. Both hyperglycemia and dyslipidemia are associated with PD. Therefore, the contribution of hyperglycemia in a T2DM background remains unclear in inducing neurodegeneration. In summary, T2DM is possibly related mainly to PD, and a T2DM model may be substantially suitable for studying metabolic disturbance as an early risk factor for PD. However, investigation of a direct effect of hyperglycemia on nigrostriatal degeneration would demand a straightforward model harvesting mainly elevated blood glucose levels in a relatively short time.

Compared to T2DM models, the T1DM model with direct damage to insulin secretion certainly possesses a purer background. Although studies focusing on the effect of hyperglycemia caused by T1DM on neurodegenerative diseases are very limited[51, 58], cognitive impairments and structural alterations in the brain are common in adults with T1DM[59], suggesting the close relation between T1DM and neurodegeneration. In a prospective study, patients with T1DM showed a substantial reduction in limb flexibility and spontaneous movements, associated with brain dysfunction[60]. The direct damage of insulin-producing β-cell provides T1DM with hyperglycemia as its main metabolic pathology[61]. The effects of hyperglycemia-induced brain function deficits come from an immediate result of the increased glucose levels[62]. Therefore, in our work, we chose the T1DM model to emphasize the direct effect of hyperglycemia on nigral neuron and PD protein pathology.

4.2. The mechanisms of hyperglycemia-induced PD progression

In the present study, we have proposed neuroinflammation as the major mechanistic process from hyperglycemia to PD, linking T1DM and PD on a cellular level. In T1DM, how does hyperglycemia cause neuroinflammation? High blood glucose levels can saturate mitochondrial respiration in endothelial cells, astrocytes and pericytes, which in turn promotes reactive oxygen species (ROS) production and oxidative stress[63, 64]. When a high glucose level is maintained for a long time, enhanced ROS and inflammatory cytokines may interrupt the integrity of BBB[33]. The integrity of the BBB is essential to maintain the brain environment homeostasis by limiting the pass-through of peripheral immune cells and toxins space[65]. Upon the penetration of peripheral proinflammatory factors, microglia are activated, and neuroinflammation occurs. Neuroinflammation has been commonly recognized as a crucial feature of PD pathogenesis[66]. Therefore, a chain of events as described above constitute the whole mechanistic process of hyperglycemia-induced neuronal damages. Although in our study, we chose only neuroinflammation, which is only one point on the mechanistic chain, to elucidate the molecular and cellular events from T1DM to PD, the underlying cellular changes such as increased oxidative stress, overproduction of ROS, mitochondrial dysfunction and leakage on the BBB are all present. Further researches on the exact point of action of high levels of blood glucose can be very informative.

4.3. Hyperglycemia-potential risk factor but not direct initiator in PD pathogenesis

In our study, we did not observe α-syn aggregation in diabetic WT mice. This is consistent with the behavioral results and the TH downregulation. STZ-induced T1DM model we utilized is an acute islet injury model rather than a slowly progressive diabetic model, making it less likely to recapitulate the slow, progressive aggregation of α-syn in WT mice. Hyperglycemia on its own fails to induce the protein pathology of PD. Previous studies have shown T2DM triggers α-syn accumulation, aggregation and phosphorylation in pancreatic β cells and the brain[28, 29, 67]. Impaired insulin signaling in T2DM causes neuronal insulin resistance in patients, which promotes α-syn accumulations[37, 68]. In the T2DM background, the joint effects of multiple metabolic deficiencies, including hyperglycemia and insulin

resistance, lead to pathological protein changes. Hyperglycemia alone, at least in the short term, is not able to initiate neurodegeneration. However, hyperglycemia still serves as a risk factor to PD from the protein pathology point of view. In our PD mice, hyperglycemia can accelerate the already existing PD pathology. α-Syn accumulation during ageing showed more severe aggregation and phosphorylation after STZ injection than the vehicle groups.

5. Conclusion

In conclusion, our finding showed that hyperglycemia aggravates PD progression. STZ-induced T1DM mice exhibited significant depletion of dopaminergic profiles, increased α-syn accumulation and phosphorylation in the nigrostriatal system and deficiency in motor performances. In addition, we observed severe neuroinflammation in the α-syn+STZ mice and concluded neuroinflammation as one of the mechanisms contributing to hyperglycemia-induced nigrostriatal degeneration. Overall, our study bridges metabolic disorders and neurodegeneration from a cellular mechanism point of view, providing referential value to investigating the etiology of PD and age-related metabolic and neuronal disorders.

Abbreviations

α-syn	alpha-synuclein	MHC class II	major histocompatibility complex Class II
AD	Alzheimer's disease	OFT	open field test
ANOVA	analysis of variance	PBS	phosphate buffer saline
BAC	bacterial artificial chromosome	PD	Parkinson's disease
BBB	blood-brain barrier	PFA	paraformaldehyde
CE	coefficient of error	PMSF	phenylmethylsulfonyl fluoride
CNS	central nervous system	pS129-α-syn	serine 129 phosphorylated α-syn
DAB	diaminobenzidine	PVDF	polyvinylidene difluoride membranes
DAPI	2-(4-Amidinophenyl)-6-indolecarbamidine dihydrochloride	ROS	reactive oxygen species
		S129	Serine 129
DAT	dopamine transporter	SEM	standard error of the mean
DM	diabetes mellitus	SN	substantia nigra
GFAP	glial fibrillary acidic protein	SNpc	substantia nigra pars compacta
GFP	green fluorescent protein	STZ	streptozotocin
HRP	horseradish peroxidase	T1DM	type 1 diabetes mellitus
IAPP	islet amyloid polypeptide	T2DM	type 2 diabetes mellitus
Iba-1	ionized calcium binding adapter molecule 1	TBST	tris buffered saline with Tween-20
		TNF-α	tumor necrosis factor-alpha
i.p.	intraperitoneal injection	TH	tyrosine hydroxylase
LBs	Lewy Bodies	VTA	ventral tegmental area
IL-1β	interleukin-1 beta	WT	wild type
IL-6	interleukin-6		

Declarations

Acknowledgement

We thank Dr. Cong Feng, Dr. Xiao-yan Gao, Dong-yan Song, Na Cui, Sheng Yang for their excellent intellectual inputs.

Authors' contributions

J-Y.L. and W.L. designed and supervised the project; Y-Q.L., L.Y., S.Y., H-W.D., J-H.S. and Z-P.H. performed research, analyzed the data; Y-Q.L., Y-L., J-Y.L. and W.L. interpreted data and wrote the manuscript. All authors edited and approved the paper.

Funding

Financial supports by the National Natural Science Foundation of China (81430025, 31800898, and U1801681 to J-Y.L. and W.L.) and the Key Field Research Development Program of Guangdong Province (2018B030337001); and The Swedish Research Council (2019-01551), EU-JPND research (αSynProtec and REfrAME) and EU-Horizon2020 (MSCA-ITN-2016, SynDeGen), ParkinsonFonden, the Strategic Research Area Multipark (Multidisciplinary research in Parkinson's disease at Lund University) and Svenska Sällskapet för Medicinsk Forskning (SSMF, P18-0194).

Availability of data and materials

All data generated or analyzed during this study are included in this published article (and its supplementary information files).

Ethics approval

Ethical approval was granted from the Research Ethics Committee of China Medical University, Shenyang, China. All involving animal experiments and procedures were approved by the Ethical Committees for the use of laboratory animals at China Medical University, China.

Consent for publication

All authors have read the manuscript and indicated consent for publication.

Competing of interests

The authors declare that they have no competing interests.

References

1. Poewe W, Seppi K, Tanner CM, Halliday GM, Brundin P, Volkmann J, et al. Parkinson disease. Nat Rev Dis Primers. 2017;3:17013.
2. Spillantini MG, Schmidt ML, Lee VM, Trojanowski JQ, Jakes R, Goedert M. Alpha-synuclein in Lewy bodies. Nature. 1997;388:839–40.
3. Zhao Y, Yang G. Potential of extracellular vesicles in the Parkinson's disease - Pathological mediators and biomarkers. Neurochem Int. 2021;144:104974.

4. Kin K, Yasuhara T, Kameda M, Date I. Animal Models for Parkinson's Disease Research: Trends in the 2000s. Int J Mol Sci 2019; 20.
5. Biosa A, Outeiro TF, Bubacco L, Bisaglia M. Diabetes Mellitus as a Risk Factor for Parkinson's Disease: a Molecular Point of View. Mol Neurobiol. 2018;55:8754–63.
6. Thomas CC, Philipson LH. Update on diabetes classification. Med Clin North Am. 2015;99:1–16.
7. Zaccardi F, Webb DR, Yates T, Davies MJ. Pathophysiology of type 1 and type 2 diabetes mellitus: a 90-year perspective. Postgrad Med J. 2016;92:63–9.
8. Lind M, Svensson AM, Kosiborod M, Gudbjornsdottir S, Pivodic A, Wedel H, et al. Glycemic control and excess mortality in type 1 diabetes. N Engl J Med. 2014;371:1972–82.
9. Katsarou A, Gudbjornsdottir S, Rawshani A, Dabelea D, Bonifacio E, Anderson BJ, et al. Type 1 diabetes mellitus. Nat Rev Dis Primers. 2017;3:17016.
10. Daems C, Welsch S, Boughaleb H, Vanderroost J, Robert A, Sokal E, et al. Early Treatment with Empagliflozin and GABA Improves beta-Cell Mass and Glucose Tolerance in Streptozotocin-Treated Mice. J Diabetes Res 2019; 2019: 2813489.
11. Maahs DM, West NA, Lawrence JM, Mayer-Davis EJ. Epidemiology of type 1 diabetes. Endocrinol Metab Clin North Am. 2010;39:481–97.
12. Ingelfinger JR, Jarcho JA. Increase in the Incidence of Diabetes and Its Implications. N Engl J Med. 2017;376:1473–4.
13. Arif B, Grunewald A, Fatima A, Ramirez A, Ali A, Bruggemann N, et al. An unusual neurological syndrome of crawling gait, dystonia, pyramidal signs, and limited speech. Mov Disord. 2011;26:2279–83.
14. Mittal K, Katare DP. Shared links between type 2 diabetes mellitus and Alzheimer's disease: A review. Diabetes Metab Syndr. 2016;10:144–9.
15. Athauda D, Foltynie T. Insulin resistance and Parkinson's disease: A new target for disease modification? Prog Neurobiol. 2016;145-146:98–120.
16. Yang YW, Hsieh TF, Li CI, Liu CS, Lin WY, Chiang JH, et al. Increased risk of Parkinson disease with diabetes mellitus in a population-based study. Med (Baltim). 2017;96:e5921.
17. D'amelio M, Ragonese P, Callari G, Di Benedetto N, Palmeri B, Terruso V, et al. Diabetes preceding Parkinson's disease onset. A case-control study. Parkinsonism Relat Disord. 2009;15:660–4.
18. Palacios N, Gao X, Mccullough ML, Jacobs EJ, Patel AV, Mayo T, et al. Obesity, diabetes, and risk of Parkinson's disease. Mov Disord. 2011;26:2253–9.
19. Miyake Y, Tanaka K, Fukushima W, Sasaki S, Kiyohara C, Tsuboi Y, et al. Case-control study of risk of Parkinson's disease in relation to hypertension, hypercholesterolemia, and diabetes in Japan. J Neurol Sci. 2010;293:82–6.
20. Kotagal V, Albin RL, Muller ML, Koeppe RA, Frey KA, Bohnen NI. Diabetes is associated with postural instability and gait difficulty in Parkinson disease. Parkinsonism Relat Disord. 2013;19:522–6.

21. Yue X, Li H, Yan H, Zhang P, Chang L, Li T. Risk of Parkinson Disease in Diabetes Mellitus: An Updated Meta-Analysis of Population-Based Cohort Studies. Med (Baltim). 2016;95:e3549.
22. Han C, Lu Y, Cheng H, Wang C, Chan P. The impact of long-term exposure to ambient air pollution and second-hand smoke on the onset of Parkinson disease: a review and meta-analysis. Public Health. 2020;179:100–10.
23. Eze IC, Hemkens LG, Bucher HC, Hoffmann B, Schindler C, Kunzli N, et al. Association between ambient air pollution and diabetes mellitus in Europe and North America: systematic review and meta-analysis. Environ Health Perspect. 2015;123:381–9.
24. Bosco D, Plastino M, Cristiano D, Colica C, Ermio C, De Bartolo M, et al. Dementia is associated with insulin resistance in patients with Parkinson's disease. J Neurol Sci. 2012;315:39–43.
25. Mucibabic M, Steneberg P, Lidh E, Straseviciene J, Ziolkowska A, Dahl U, et al. alpha-Synuclein promotes IAPP fibril formation in vitro and beta-cell amyloid formation in vivo in mice. Sci Rep. 2020;10:20438.
26. De Pablo-Fernandez E, Goldacre R, Pakpoor J, Noyce AJ, Warner TT. Association between diabetes and subsequent Parkinson disease: A record-linkage cohort study. Neurology. 2018;91:e139–42.
27. Perruolo G, Viggiano D, Fiory F, Cassese A, Nigro C, Liotti A, et al. Parkinson-like phenotype in insulin-resistant PED/PEA-15 transgenic mice. Sci Rep. 2016;6:29967.
28. Wang L, Zhai YQ, Xu LL, Qiao C, Sun XL, Ding JH, et al. Metabolic inflammation exacerbates dopaminergic neuronal degeneration in response to acute MPTP challenge in type 2 diabetes mice. Exp Neurol. 2014;251:22–9.
29. Sun Y, Guo C, Yuan L, Li W, Wang ZY, Yue F, et al. Cynomolgus Monkeys With Spontaneous Type-2-Diabetes-Mellitus-Like Pathology Develop Alpha-Synuclein Alterations Reminiscent of Prodromal Parkinson's Disease and Related Diseases. Front Neurosci. 2020;14:63.
30. Wakabayashi T, Yamaguchi K, Matsui K, Sano T, Kubota T, Hashimoto T, et al. Differential effects of diet- and genetically-induced brain insulin resistance on amyloid pathology in a mouse model of Alzheimer's disease. Mol Neurodegener. 2019;14:15.
31. Van Dyken P, Lacoste B. Impact of Metabolic Syndrome on Neuroinflammation and the Blood-Brain Barrier. Front Neurosci. 2018;12:930.
32. Wen L, Duffy A. Factors Influencing the Gut Microbiota, Inflammation, and Type 2 Diabetes. J Nutr. 2017;147:1468S–1475S.
33. Elmarakby AA, Sullivan JC. Relationship between oxidative stress and inflammatory cytokines in diabetic nephropathy. Cardiovasc Ther. 2012;30:49–59.
34. Nayak S, Soon SQ, Kunjal R, Ramadoo R, Baptiste O, Persad J, et al. Relationship between adiponectin, inflammatory markers and obesity in type 2 diabetic and non-diabetic Trinidadians. Arch Physiol Biochem. 2009;115:28–33.
35. Thundyil J, Lim KL. DAMPs and neurodegeneration. Ageing Res Rev. 2015;24:17–28.

36. Hickman S, Izzy S, Sen P, Morsett L, El Khoury J. Microglia in neurodegeneration. Nat Neurosci. 2018;21:1359–69.
37. Bassil F, Canron MH, Vital A, Bezard E, Li Y, Greig NH, et al. Insulin resistance and exendin-4 treatment for multiple system atrophy. Brain. 2017;140:1420–36.
38. Kacirova M, Zmeskalova A, Korinkova L, Zelezna B, Kunes J, Maletinska L. Inflammation: major denominator of obesity, Type 2 diabetes and Alzheimer's disease-like pathology? Clin Sci (Lond). 2020;134:547–70.
39. Hansen C, Bjorklund T, Petit GH, Lundblad M, Murmu RP, Brundin P, et al. A novel alpha-synuclein-GFP mouse model displays progressive motor impairment, olfactory dysfunction and accumulation of alpha-synuclein-GFP. Neurobiol Dis. 2013;56:145–55.
40. Chen QQ, Haikal C, Li W, Li MT, Wang ZY, Li JY. Age-dependent alpha-synuclein accumulation and aggregation in the colon of a transgenic mouse model of Parkinson's disease. Transl Neurodegener. 2018;7:13.
41. Zhong CB, Chen QQ, Haikal C, Li W, Svanbergsson A, Diepenbroek M, et al. Age-Dependent Alpha-Synuclein Accumulation and Phosphorylation in the Enteric Nervous System in a Transgenic Mouse Model of Parkinson's Disease. Neurosci Bull. 2017;33:483–92.
42. Wang Z, Dohle C, Friemann J, Green BS, Gleichmann H. Prevention of high- and low-dose STZ-induced diabetes with D-glucose and 5-thio-D-glucose. Diabetes. 1993;42:420–8.
43. Liang Y, Chen C, Xia B, Wu W, Tang J, Chen Q, et al. Neuroprotective Effect of Echinacoside in Subacute Mouse Model of Parkinson's Disease. Biomed Res Int 2019; 2019: 4379639.
44. Gou DH, Huang TT, Li W, Gao XD, Haikal C, Wang XH, et al. Inhibition of copper transporter 1 prevents alpha-synuclein pathology and alleviates nigrostriatal degeneration in AAV-based mouse model of Parkinson's disease. Redox Biol. 2021;38:101795.
45. Decressac M, Ulusoy A, Mattsson B, Georgievska B, Romero-Ramos M, Kirik D, et al. GDNF fails to exert neuroprotection in a rat alpha-synuclein model of Parkinson's disease. Brain. 2011;134:2302–11.
46. Baquet ZC, Williams D, Brody J, Smeyne RJ. A comparison of model-based (2D) and design-based (3D) stereological methods for estimating cell number in the substantia nigra pars compacta (SNpc) of the C57BL/6J mouse. Neuroscience. 2009;161:1082–90.
47. Sanchez-Guajardo V, Febbraro F, Kirik D, Romero-Ramos M. Microglia acquire distinct activation profiles depending on the degree of alpha-synuclein neuropathology in a rAAV based model of Parkinson's disease. PLoS One. 2010;5:e8784.
48. Bonnevie-Nielsen V, Steffes MW, Lernmark A. A major loss in islet mass and B-cell function precedes hyperglycemia in mice given multiple low doses of streptozotocin. Diabetes. 1981;30:424–9.
49. Fujiwara H, Hasegawa M, Dohmae N, Kawashima A, Masliah E, Goldberg MS, et al. alpha-Synuclein is phosphorylated in synucleinopathy lesions. Nat Cell Biol. 2002;4:160–4.
50. Izco M, Blesa J, Verona G, Cooper JM, Alvarez-Erviti L. Glial activation precedes alpha-synuclein pathology in a mouse model of Parkinson's disease. Neurosci Res. 2021;170:330–40.

51. Perez-Taboada I, Alberquilla S, Martin ED, Anand R, Vietti-Michelina S, Tebeka NN, et al. Diabetes Causes Dysfunctional Dopamine Neurotransmission Favoring Nigrostriatal Degeneration in Mice. Mov Disord. 2020;35:1636–48.
52. Aviles-Olmos I, Limousin P, Lees A, Foltynie T. Parkinson's disease, insulin resistance and novel agents of neuroprotection. Brain. 2013;136:374–84.
53. Bassil F, Fernagut PO, Bezard E, Meissner WG, Insulin. IGF-1 and GLP-1 signaling in neurodegenerative disorders: targets for disease modification? Prog Neurobiol. 2014;118:1–18.
54. Chen C, Cohrs CM, Stertmann J, Bozsak R, Speier S. Human beta cell mass and function in diabetes: Recent advances in knowledge and technologies to understand disease pathogenesis. Mol Metab. 2017;6:943–57.
55. Bulut T, Demirel F, Metin A. The prevalence of dyslipidemia and associated factors in children and adolescents with type 1 diabetes. J Pediatr Endocrinol Metab. 2017;30:181–7.
56. Athyros VG, Doumas M, Imprialos KP, Stavropoulos K, Georgianou E, Katsimardou A, et al. Diabetes and lipid metabolism. Hormones (Athens). 2018;17:61–7.
57. Heydemann A. An Overview of Murine High Fat Diet as a Model for Type 2 Diabetes Mellitus. J Diabetes Res 2016; 2016: 2902351.
58. Renaud J, Bassareo V, Beaulieu J, Pinna A, Schlich M, Lavoie C, et al. Dopaminergic neurodegeneration in a rat model of long-term hyperglycemia: preferential degeneration of the nigrostriatal motor pathway. Neurobiol Aging. 2018;69:117–28.
59. Shalimova A, Graff B, Gasecki D, Wolf J, Sabisz A, Szurowska E, et al. Cognitive Dysfunction in Type 1 Diabetes Mellitus. J Clin Endocrinol Metab. 2019;104:2239–49.
60. Moheet A, Mangia S, Seaquist ER. Impact of diabetes on cognitive function and brain structure. Ann N Y Acad Sci. 2015;1353:60–71.
61. Gillespie KM. Type 1 diabetes: pathogenesis and prevention. CMAJ. 2006;175:165–70.
62. Penicaud L, Leloup C, Fioramonti X, Lorsignol A, Benani A. Brain glucose sensing: a subtle mechanism. Curr Opin Clin Nutr Metab Care. 2006;9:458–62.
63. Liyanagamage D, Martinus RD. Role of Mitochondrial Stress Protein HSP60 in Diabetes-Induced Neuroinflammation. Mediators Inflamm 2020; 2020: 8073516.
64. Wang J, Li G, Wang Z, Zhang X, Yao L, Wang F, et al. High glucose-induced expression of inflammatory cytokines and reactive oxygen species in cultured astrocytes. Neuroscience. 2012;202:58–68.
65. Zhao Z, Nelson AR, Betsholtz C, Zlokovic BV. Establishment and Dysfunction of the Blood-Brain Barrier. Cell. 2015;163:1064–78.
66. De Lella Ezcurra AL, Chertoff M, Ferrari C, Graciarena M, Pitossi F. Chronic expression of low levels of tumor necrosis factor-alpha in the substantia nigra elicits progressive neurodegeneration, delayed motor symptoms and microglia/macrophage activation. Neurobiol Dis. 2010;37:630–40.

67. Martinez-Valbuena I, Amat-Villegas I, Valenti-Azcarate R, Carmona-Abellan MDM, Marcilla I, Tunon MT, et al. Interaction of amyloidogenic proteins in pancreatic beta cells from subjects with synucleinopathies. Acta Neuropathol. 2018;135:877–86.

68. Gao S, Duan C, Gao G, Wang X, Yang H. Alpha-synuclein overexpression negatively regulates insulin receptor substrate 1 by activating mTORC1/S6K1 signaling. Int J Biochem Cell Biol. 2015;64:25–33.

Figures

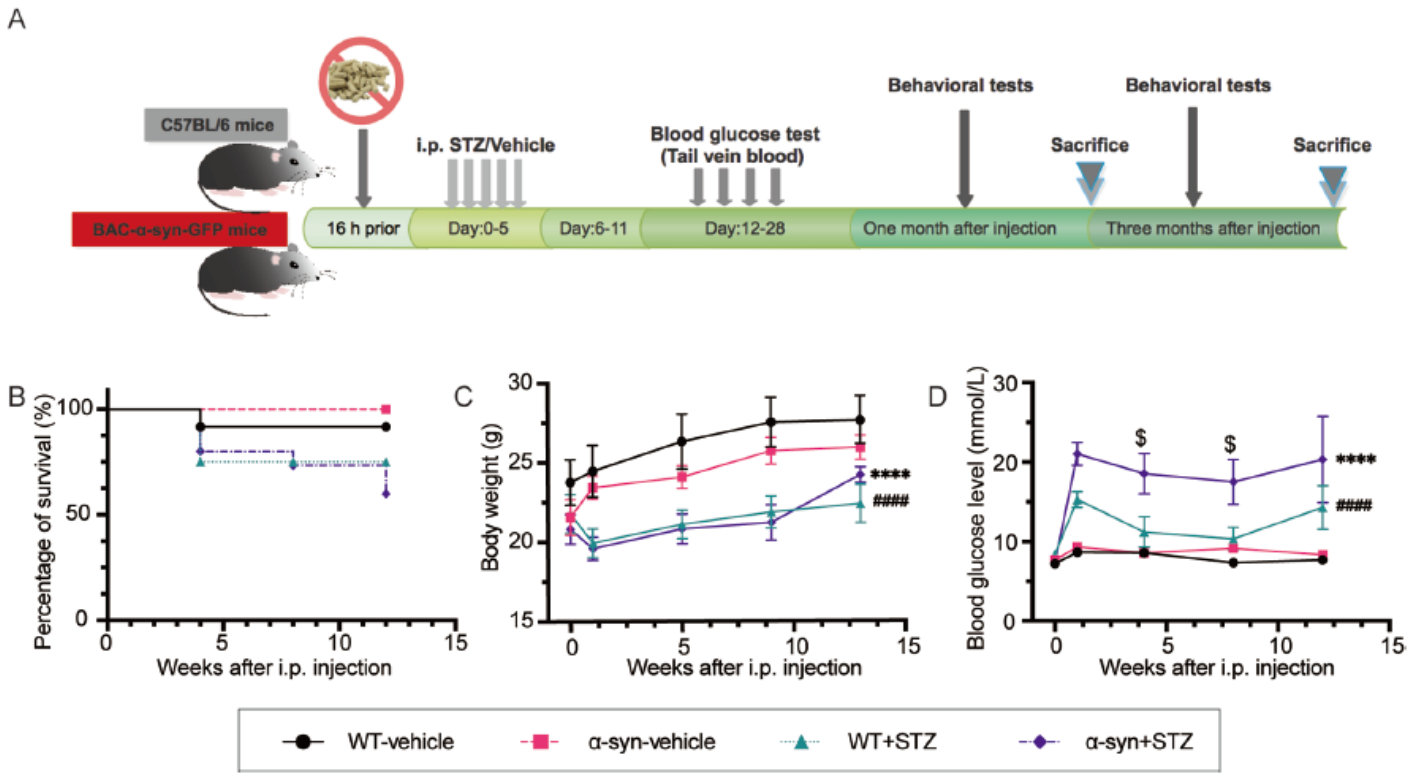

Figure 1

STZ treatment reduced the body weight and induced more severe hyperglycemia in α-syn-overexpression mice. (A) Schematic drawings showed the experimental design. Both WT and BAC-α-syn-GFP mice were i.p. injected with STZ or vehicle. In the process, body weight and blood glucose levels were routinely monitored. The mice were respectively subjected to behavioral tests one month and three months after injection. (B) Percentage of survival 12 weeks after STZ i.p. injection. (C-D) Body weight and blood glucose alterations during the months after STZ i.p. injection. ****P<0.0001 in α-syn+STZ vs α-syn-vehicle, ####P<0.0001 in WT+STZ vs WT-vehicle, $P<0.05 in WT+STZ vs α-syn+STZ.

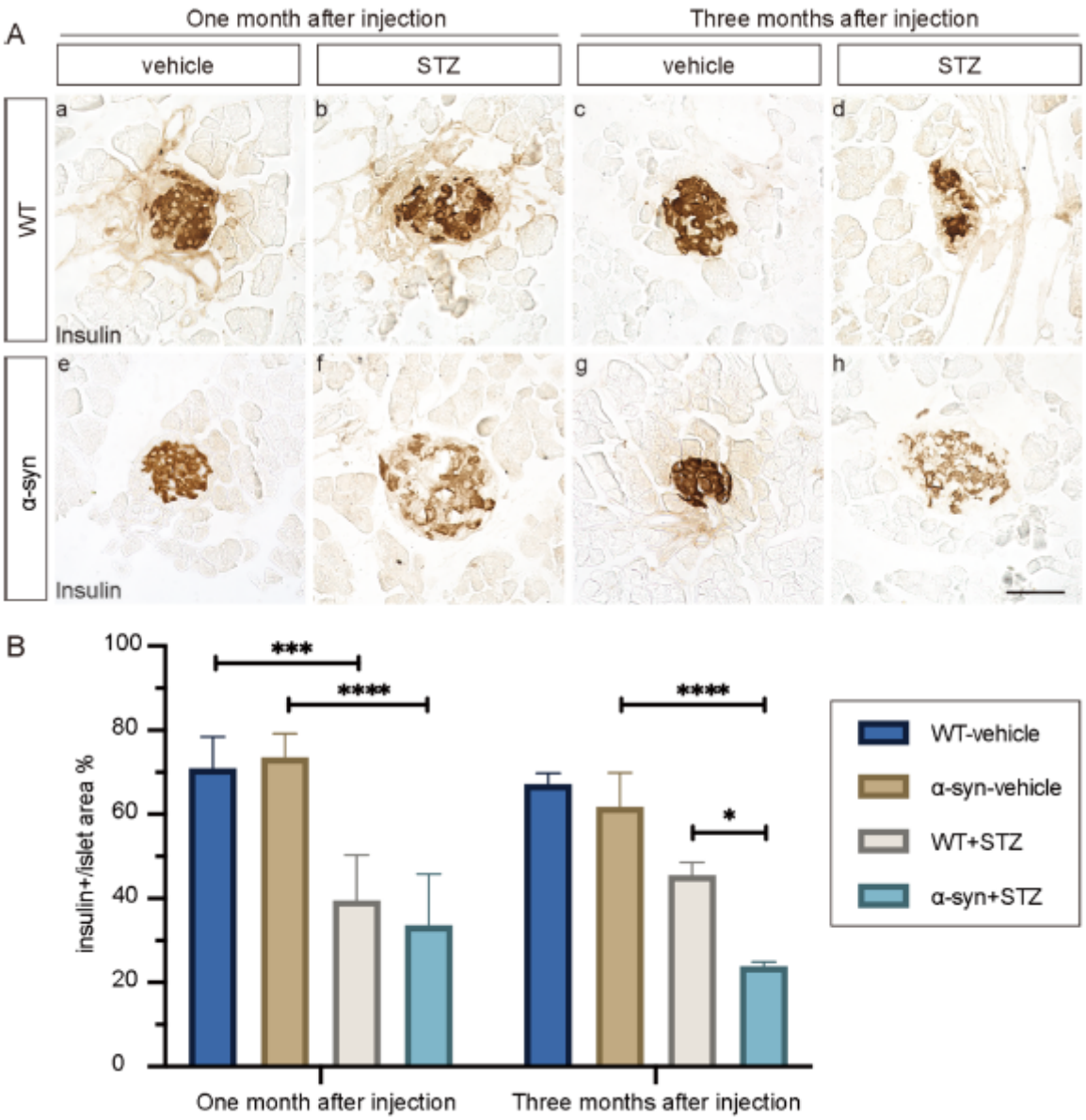

Figure 2

STZ treatment exacerbated more severe structural damage of islets in α-syn-overexpression mice compared to WT. (A) Representative microscopic images of immunohistochemical staining with antibody specifically against insulin at one (a, b, e, f) and three months (c, d, g, h) after injection in the pancreatic islets of WT-vehicle (a, c), WT+STZ (b, d), α-syn-vehicle (e, g) and α-syn+STZ (f, h) groups. (B) Quantification of average ratio of islet β-cell area to total islet area (insulin+/islet area%) in pancreases of WT and BAC-α-syn-GFP mice i.p. injected with STZ and vehicle. Scale bar: (a-h), 50 μm. *P<0.05, ***P<0.001, ****P<0.0001.

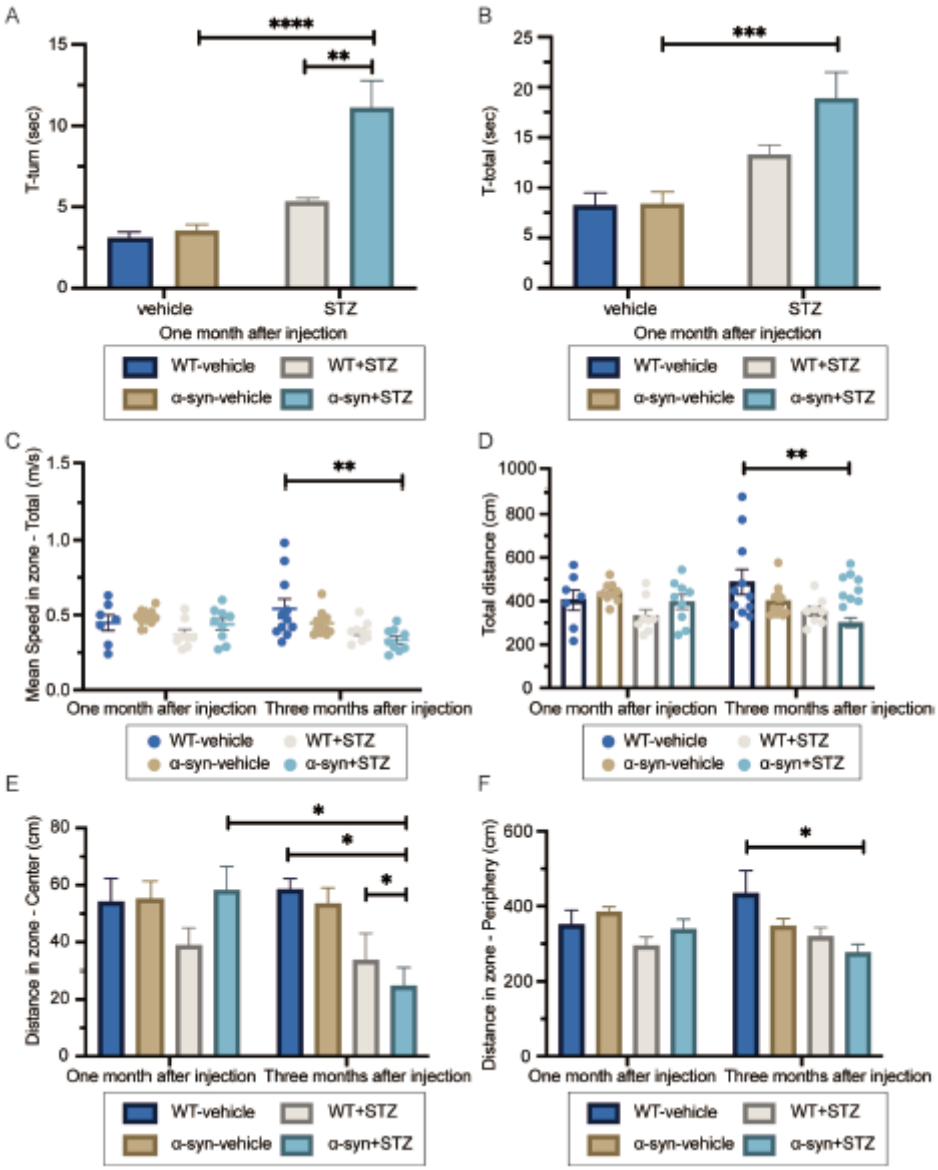

Figure 3

Long-term hyperglycemia induced motor deficits in α-syn-overexpression mice. Motor performance evaluation one and three months after injection using pole test (A-B) and OFT (C-F). T-turn (A) and T-total (B) increased in STZ treated group compared to vehicle. (C-F) The OFT was used to access the spontaneous activity of mice. The mean speed in total zone (C), total distance (D), distance in center zone (E) and distance in periphery zone (F)were different between α-syn+STZ and WT-vehicle groups. *P<0.05, **P<0.01, ***P<0.001, ****P<0.0001.

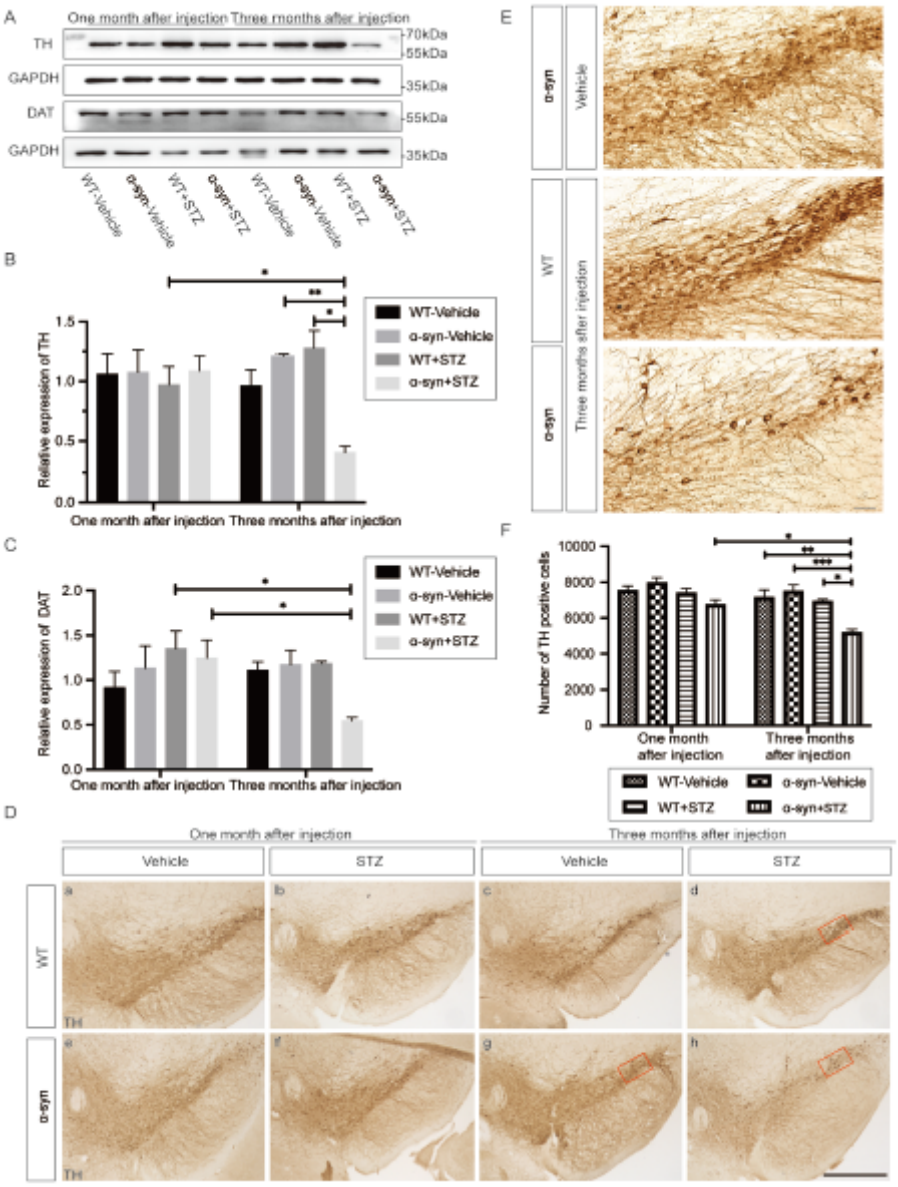

Figure 4

Long-term hyperglycemia caused degeneration of dopaminergic neuronal profile in α-syn-overexpression mice. (A) Western blot analyses of TH and DAT protein levels in mouse SNpc. (B-C) Quantification of relative expression of TH and DAT was performed by intensity measurement. (D) Representative photomicrographs of coronal mesencephalic sections showing immunohistochemical staining of TH in the SN of both WT and BAC-α-syn-GFP mice injected with STZ and vehicle. (E) High-magnification images correspond to the selected areas indicated by a rectangle in (d), (g), and (h). (F) Quantitative analyses of TH positive neurons determined by stereology in the midbrain region. Scale bar: (D-E), 50 μm. *P<0.05, **P<0.01, ***P<0.001.

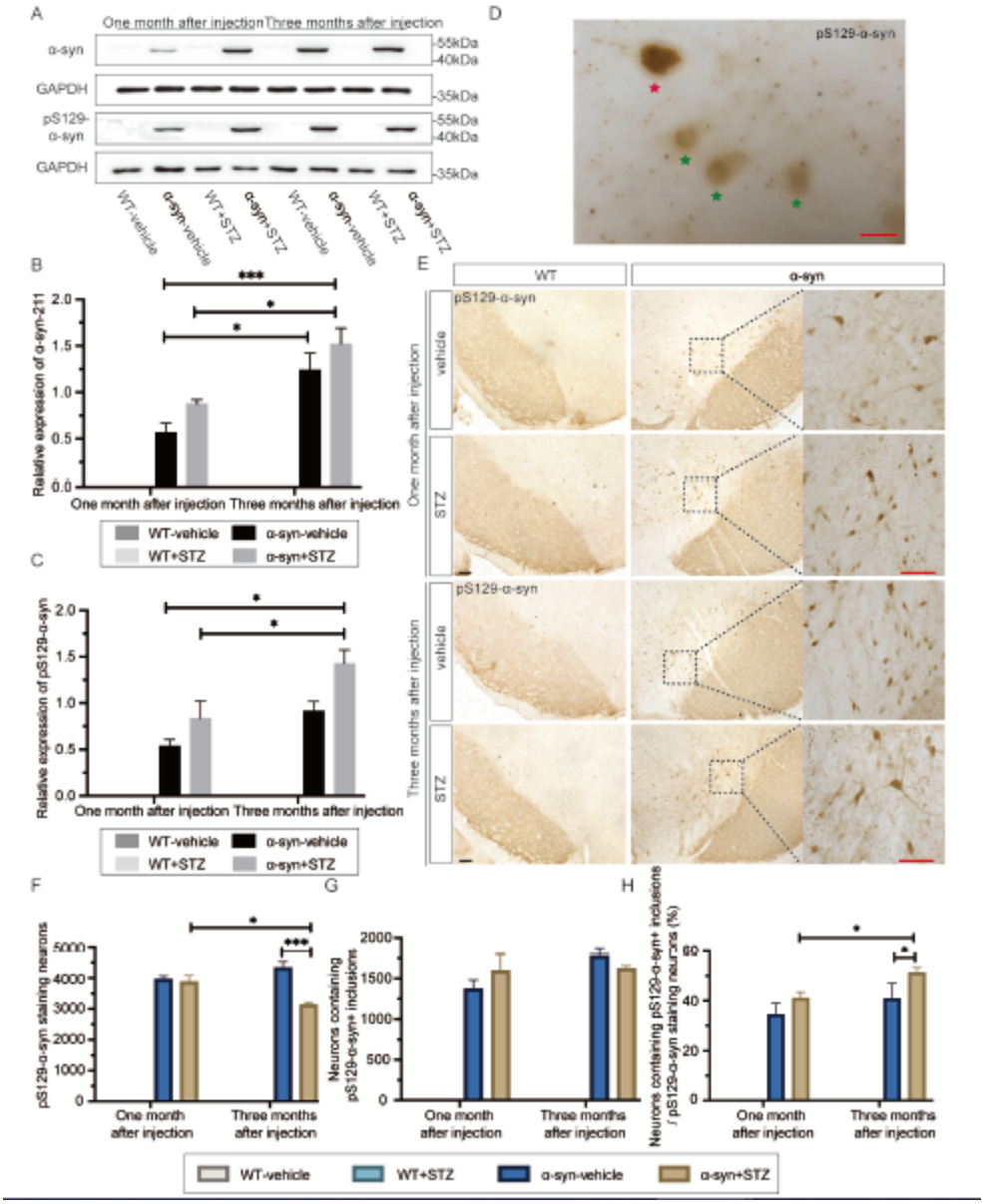

Figure 5

Hyperglycemia increased α-syn aggregation and phosphorylation in the nigrostriatal system in α-syn-overexpression mice. (A) Western blot analyses of α-syn and phosphorylated α-syn (pS129) levels in mouse SN. (B-C) Quantification of relative expression of α-syn and pS129-α-syn was performed by intensity measurement. (D) Three-dimensional picture (z-axis with 20 μm thickness) of two different types of pS129-α-syn positive neurons in SN. (red stellates marked the neuron containing pS129-α-syn+ inclusions; green stellates marked the neurons without pS129-α-syn+ inclusions). (E) Representative immunohistochemical images of pS129-α-syn in the SN of WT and BAC-α-syn-GFP mice at one and three months after injection. The pictures in the right column show higher magnification images of the rectangle area in the middle column. (F-H) Stereological quantification the number of pS129-α-syn staining neurons in the SN (red + green stellates) in (F), neurons containing pS129-α-syn+ inclusions (red stellates) in (G) and the proportion of neurons containing pS129-α-syn+ inclusions in all pS129-α-syn

staining neurons (red/red + green stellates) in (H). Image scale bars: (D), 10 μm; (E) left column, 200 μm; right column, 50 μm. *P<0.05, **P<0.01, ***P<0.001.

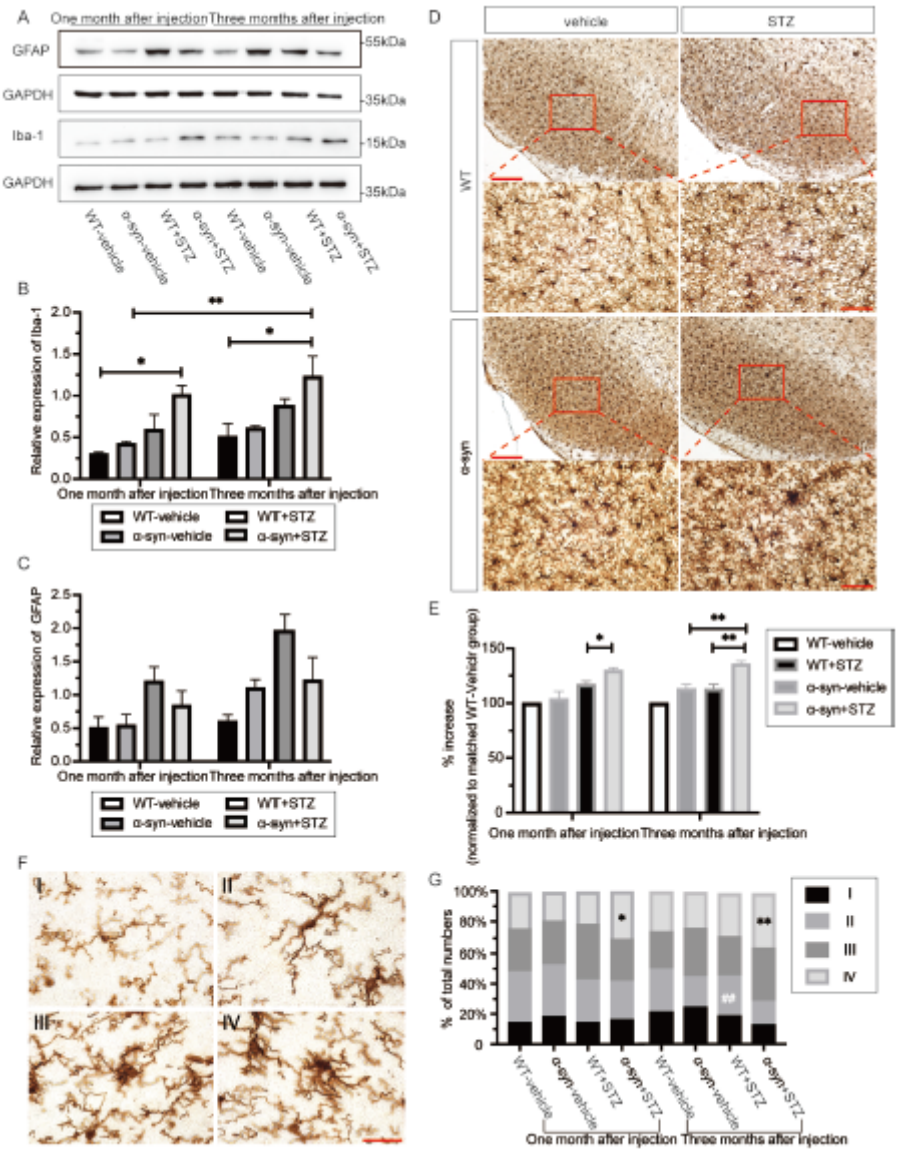

Figure 6

Hyperglycemia promoted neuroinflammation in BAC-α-syn-GFP mice. (A) Representative immunoblot of Iba-1 and GFAP in western blot. (B-C) Quantification of relative expression of Iba-1 and GFAP was performed by intensity measurement. (D) Representative immunohistochemical Iba-1 staining of the SN of mice. (E) Number of SN microglia were analyzed at each time point. Numbers were normalized to the number of microglia in the WT-vehicle group mice at each time point. (F) The morphology of SN microglia was analyzed at each time point. The representative images of morphologies of microglia at four different activation stages (I, II, III, IV). (G) The bar chart shows the proportion of four types of microglia based on different morphology. Image scale bars: (D), left column, 100 μm; right column, 50 μm; (F), 20 μm. *P<0.05, **P<0.01 in (B) and (C). *P<0.05 and **P<0.01 in α-syn+STZ vs α-syn-vehicle in stage IV at one and three months after injection; ##P<0.01 in WT+STZ vs α-syn+STZ n stage II at three months after injection in (G).

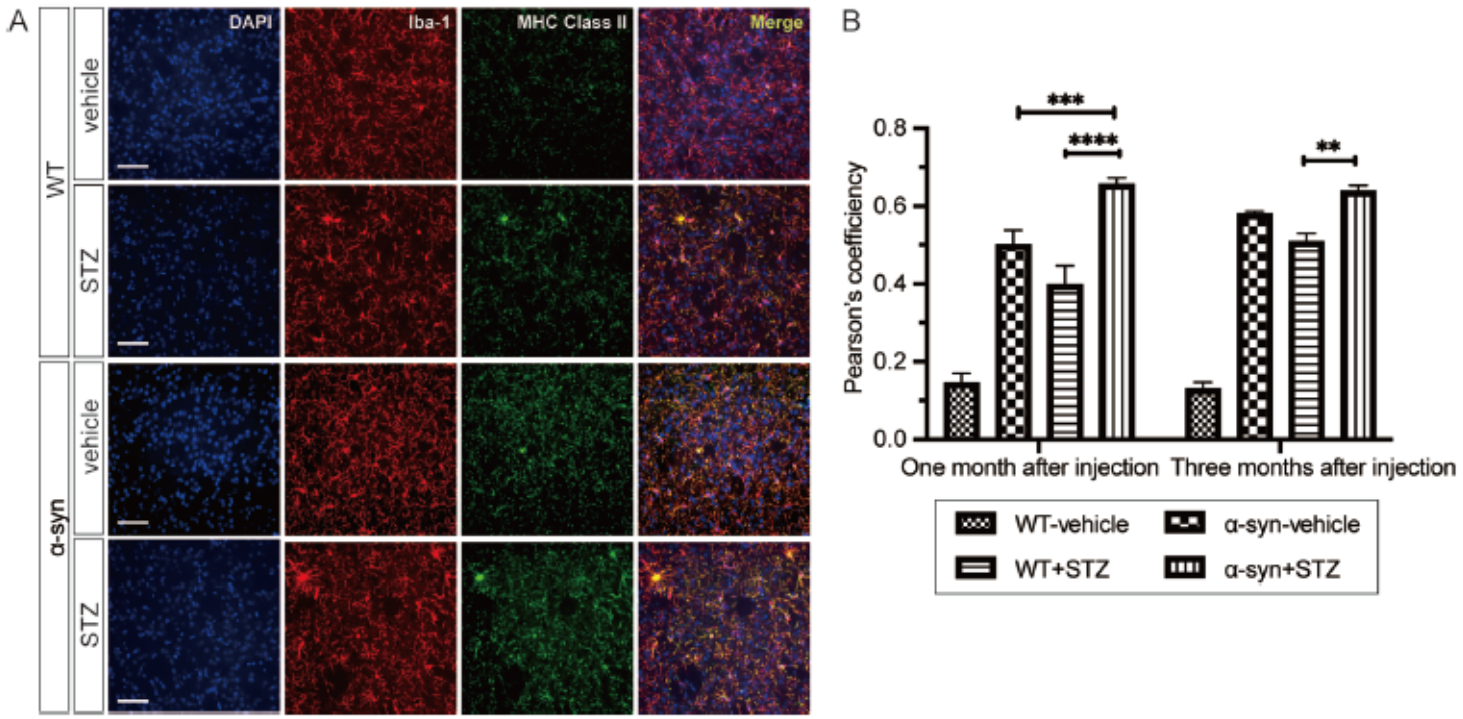

Figure 7

Co-localization of Iba-1 and MHC class II in the striatum of the mice. (A) Representative images of double-immunofluorescence staining of MHC class II and Iba-1 in the striatum of WT and BAC-α-syn-GFP mice with vehicle and STZ injection. (B) Pearson's co-efficiency of co-localization between Iba-1 and MHC class II in the striatum. Images scale bars: 50 μm. **P<0.01, ***P<0.001, ****P<0.0001.

Supplementary Files

This is a list of supplementary files associated with this preprint. Click to download.

- Additionalfile1.pdf